Theoretical Models for Metal Growth in Space—Comparison to Ground Experiments

R. I. Miller*
Boeing Aerospace Company, Huntsville, Ala.
and
M. H. Johnston†
NASA Marshall Space Flight Center, Huntsville, Ala.

A mathematical model which can predict solid material properties from known melt properties and solidification environment is being developed to aid in selecting materials systems which could benefit scientifically or commercially from experimentation in space. In its present, preliminary form, the model calculates grain size and dendrite morphology from the independent process parameters ΔT (undercooling) and θ (parameter which characterizes heterogeneous nucleation). Calculations with the present model are compared to experimental data, and needed improvements in the model are described. Some theoretical problems relating to undercooling and environmentally induced solute segregation are also discussed.

Introduction

IT is commonly accepted in science and engineering that a phenomenon is not really understood until a mathematical theory of the phenomenon is developed, from which quantitative predictions can be made which agree with experimental studies of the phenomenon. This paper deals with the application of this philosophy to the phenomenon of solidification in space. More specifically, it deals with the question of how one can predict the properties of a solid from the known properties of a melt and the environment in which it solidifies. As will be seen, one of the more important variables in the theories pertaining to such a prediction is the melt undercooling ΔT, the difference between the equilibrium melting temperature of the material and the actual temperature in the melt as solidification starts. Another important variable, which before the era of space processing research was thought of as a constant, is the acceleration vector acting on the melt, g (gravity in Earth-based processes). The space processing program has generated considerable interest in how these variables can, separately or in concert, affect the outcome of a solidification experiment in space. Hence, we will first consider two problems pertaining to the nature of undercooling and the combined effects of acceleration and undercooling, then proceed to the discussion of a mathematical model which could theoretically predict the properties of space-processed solids. The importance of such a model arises from the vast number of new materials which become theoretically possible to produce in space and from the economic necessity to have some analytical assurance that scientifically or commercially desirable properties will be obtained by solidifying a given material in space. Finally, a simple, first-cut approach to a part of a candidate material property prediction model will be derived and compared to experiment.

Presented as Paper 77-164 at the AIAA 15th Aerospace Sciences Meeting, Los Angeles, Calif., Jan. 24-26, 1977; submitted Feb. 1, 1977; revision received Sept. 26, 1977.

Index categories: Space Processing; Materials, Properties of; Thermal Modeling and Analysis.

*Physicist, Nuclear & Space Physics Department. Currently, Theoretical Physicist, U.S. Army Missile Research and Development Command, Redstone Arsenal, Ala. Member AIAA.

†Materials Engineer, Metallic Materials Division, Materials and Processes Laboratory.

Relation of Undercooling to Material Properties

The undercooling of liquids is of considerable importance in industrial solidification processes[1,2] in the study of the liquid-solid transition[3-9] and as an interesting phenomenon in its own right.[10-13] The most extensive experimental work applicable to this subject is the study of maximum undercooling and homogeneous nucleation performed 25 years ago by Turnbull,[8,9] and his data are still the most widely quoted in the literature. The important result of Turnbull's experiments, which used the "small drop" technique to insure purity and homogeneous nucleation, was the establishment of a reproducible maximum value of undercooling, ΔT_{max}, at which each liquid material nucleates homogeneously.

The classical homogeneous nucleation rate I (nuclei/cm^3 s) is given by[5]

$$I = I_0 e^{-A^2/T(\Delta T)^2} \tag{1}$$

where, for spherical nuclei,

$$A^2 = 16\pi\sigma^3/3kS_c^2 \tag{2}$$

where T is absolute temperature, σ is the liquid-solid in-

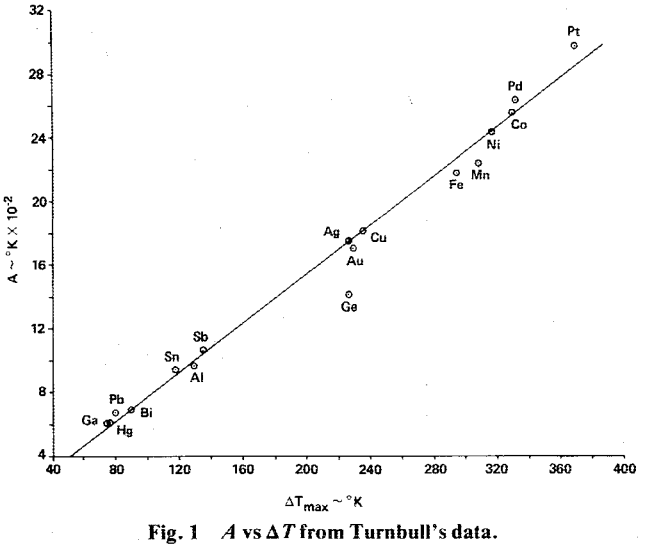

Fig. 1 A vs ΔT from Turnbull's data.

terfacial energy, S_c is the entropy of fusion, and k is Boltzmann's constant. According to Turnbull,[14] $I_0 \approx 10^{33} \approx e^{76}$ (nuclei/cm^3 s); thus,

$$I = \exp\{76 - [A^2/T(\Delta T)^2]\} \tag{3}$$

Obviously, the largest undercooling a liquid can sustain is the largest value of ΔT which leaves I in Eq. (3) essentially zero. If one takes this value of I to be less than or equal to some small, constant value ξ, then from Eq. (3)

$$\Delta T \leq A/\sqrt{T(76 - \ell n \xi)} \tag{4}$$

Therefore, the larger the value of A, or by Eq. (2) the larger the value of $\sigma^{3/2}/S_c$, for a given material, the larger undercooling $\Delta T_{\max}$ the material will sustain. (Relative to ΔT, T is practically constant.) A rigorous test of how well this classical prediction agrees with experiment must await further application of a direct technique for measuring interfacial energies, such as that developed by Glicksman and Vold.[15] This is because most published values of σ were calculated from nucleation data via Eq. (3),[4] since the Glicksman and Vold technique has not been applied to many liquids. It is no surprise, then, that values of A calculated for various liquids using Turnbull's values[8] for σ should correlate with measured ΔT_m values as well as they do in Fig. 1. Note that I and $\Delta T_{\max}$ are the variables measured by Turnbull and that $S_c = (Q/T_m)$ is the other "known" parameter used to calculate σ from the nucleation experiments.

Gravitational Segregation of Nuclei

When a multiphase alloy solidifies in a gravitational field, the settling of nuclei of the heavier phase(s) toward the bottom of the melt results in macroscopic segregation of this solute phase in the solid material. The distribution of nuclei of the heavier phase C in the melt should be described by Fick's law,

$$D\frac{dC}{dz} = -CU \tag{5}$$

where D is a "nucleus diffusion coefficient," z is the direction of the gravity vector and also the axial direction in an assumed cylindrically shaped melt, and U is nucleus settling velocity. The equation of motion for the nucleus, including friction and buoyant forces, is thus

$$M\frac{dU}{dt} = Mg - 6\pi\eta r U - \frac{4}{3}\pi r^3 \rho(z) g \tag{6}$$

where M is nucleus mass, r its radius, η the melt viscosity, and $\rho(z)$ the melt density (which is assumed to change more slowly with time than U). The acceleration due to gravity g is 980 cm/s^2. When Eq. (6) is solved for U, the result may be written as a function of $\rho(z)$ and g,

$$U(z,t) = \{1 - [\rho(z,t)/\rho_N]\}\gamma g D(1 - e^{-t/\gamma D}) \tag{7}$$

where $\rho_N = 3M/4\pi r^3$ and $\gamma = M/2kT$. For most reasonable nucleus motion, $t \gg \gamma D$, so the exponential vanishes, leaving (for slowly varying melt density)

$$U(z) = \gamma g D\{1 - [\rho(z)/\rho_N]\} \tag{8}$$

Substitution of this result into Eq. (5) and performance of the integration with respect to z lead to the integral equation

$$\ell n C = -\gamma g z + \gamma g f(z) \tag{9}$$

where

$$f(z) = \frac{1}{\rho_N}\int_0^z \rho[C(y)]dy$$

and

$$\rho[C(y)] = \frac{m_1 C(y) - m_2 C(y) + m_2 C_T}{v_1 C(y) - v_2 C(y) + v_2 C_T} \tag{10}$$

with subscripts 1 and 2 referring to solute and solvent atoms, respectively, and C_T being the total (homogeneous) melt concentration or number density. By combining constants, this can be written

$$\rho(C) = (A_3 C + m')/(A_4 C + v') \tag{11}$$

and by noting that Eq. (9) can be written $C = \exp[\gamma g(f - z)]$, one can calculate dC/dz and solve for df/dz:

$$\frac{df}{dz} = 1 + \frac{1}{\gamma g C}\frac{dC}{dz} \tag{12}$$

From the definition of $f(z)$, df/dz is also

$$\frac{df}{dz} = \frac{1}{\rho_N}\frac{A_3 C + m'}{A_4 C + v'} \tag{13}$$

Table 1 MSFC centrifuge experiment data

Sample	g level	ΔT K	V_v, %	Pb concentration in dendrites, X^D	Total Pb concentration atomic, %
2A1	1	0	27	0.710	38
3A1	1	7.5	35	0.733	43
5A1	1	8.6	37	0.737	44
1A1	1	11.34	40.5	0.745	46
1A3	3	0	46.5	0.710	47
2A3	3	6.05	49.5	0.728	49
...	3	10.8	...	0.743	...
3A3	3	11.34	56.5	0.745	53
5A3	3	14.7	59	0.755	55
4A5	5	0	50	0.710	48.5
3A5	5	1.89	...	0.715	...
2A5	5	6.05	55.5	0.728	52
1A5	5	7.0	...	0.762	...
5A5	5	8.69	60	0.737	55
7A5	5	16.44	45.5	0.760	49

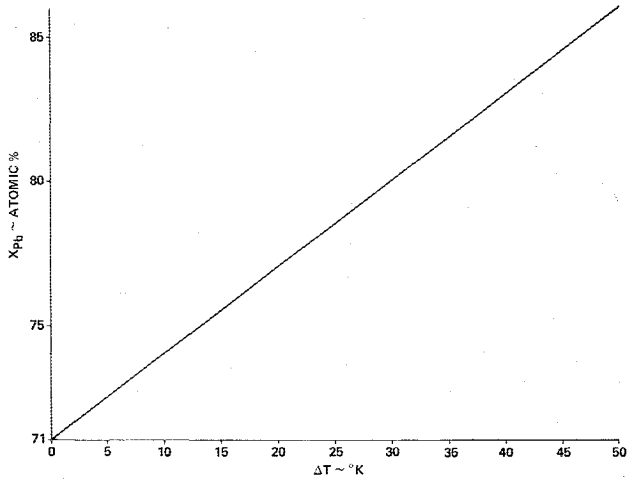

Fig. 2 Approximate atomic % Pb in dendrites that nucleate at ΔT.

Equating the right-hand sides of Eqs. (12) and (13) leads to the new differential equation

$$\frac{(A_4C+v')\,dC}{B_1C^2+B_2C}=\gamma g\,dz \tag{14}$$

with

$$B_1=(A_3/\rho_N)-A_4 \text{ and } B_2=(m'/\rho_N)-v'$$

This can be integrated directly, and applying the boundary condition that $C=C_0$ (the solute concentration equals the homogeneous concentration) at $z=0$ (the center plane of the melt), the solution obtained is

$$\left(\frac{B_1C+B_2}{B_1C_0+B_2}\right)^{[(A_4/B_1)-(v'/B_2)]}\left(\frac{C}{C_0}\right)^{(v'/B_2)}=e^{\gamma gz} \tag{15}$$

This is a complicated function of concentration and melt physical parameters. Therefore, its behavior is best illustrated by application to specific problems where all constants on the left-hand side can be evaluated.

Analysis of Undercooling and Nucleation of Lead-Tin Eutectic Material in a Centrifuge

The effects of undercooling and gravity on solidifying materials were studied through a series of experiments on Pb-Sn eutectic material by Johnston and Griner[16] at MSFC (Marshall Space Flight Center). This material was selected for the drastic difference in density of its components. In the experiments, initially solid samples of eutectic composition ($X=26$ atomic % Pb) were melted in a 1.5-cm long × 1.2-cm-diam cylindrical crucible and held in the melt state while inside a centrifuge providing a fixed centripetal acceleration equal to some integral multiple of g, 980 cm/s^2. The samples were then cooled, solidified, removed from the crucible, and analyzed metallographically to determine the volume fraction of Pb-rich dendrites at the bottom of the sample. Table 1 presents the results of these experiments together with the conversion of the volume fraction V_v to total lead atomic fraction through the Pb atomic fraction in the dendrites X^D. X^D was obtained from an approximation of the Pb-Sn phase diagram in the temperature-concentration region of interest (Fig. 2). The value of component concentration is related to atomic fraction by

$$X=C/C_T \tag{16}$$

where C_T is total melt concentration. Any concentration value is computed from

$$C_i=N_0(\rho_i/M_i) \tag{17}$$

where N_0 is Avogadro's number, ρ_i is density of the ith component, and M_i is its atomic weight. For the Pb-Sn eutectic melt, the following values were calculated: $C_T=0.35802\times10^{23}$ cm^{-3} and $C_0^{Pb}=0.1038\times10^{23}$ cm^{-3}. After obtaining other melt parameters (Table 2), the constants in Eq. (15) can be evaluated as follows:

$$v'=v_{Sn}C_T=0.96486$$

$$m'=M_{Sn}C_T=7.053 \text{ gm/cm}^3$$

$$A_4=v_{Pb}-v_{Sn}=0.335\times10^{-23}\text{cm}^3$$

$$A_3=m_{Pb}-m_{Sn}=14.69\times10^{-23}\text{gm}$$

$$B_2=m'/\rho_N-v'=-0.3442$$

$$B_1=A_3/\rho_N-A_4=0.9577\times10^{-23}\text{cm}^3$$

$$v'/B_2=-2.8$$

$$A_4/B_1=0.35$$

Equation (15) now becomes

$$\left[\frac{(0.9577\times10^{-23})C-0.3442}{-0.24479}\right]^{3.153}\left(\frac{0.1038\times10^{23}}{C}\right)^{2.803}=e^{\gamma gz} \tag{18}$$

Since the parameter γ depends on the mass, and thus the size of the nuclei which are being segregated, it therefore depends on the cube of the undercooling ΔT. Thus, to calculate the lead distribution in a sample of size -0.75 cm $< z < +0.75$ cm (Fig. 3), particular values of ΔT and g must be specified. If a value of 10 K is chosen for ΔT, curves for lead concentration distribution for different gravity levels, as shown in Fig. 4, are generated by Eq. (18). Since concentration was measured at only one position ($z=-0.75$) for

Table 2 Liquid state/solidification parameters for selected materials

Element	T_m, K	M, g/g atom	ρ, g/cm^3	v, cm^3/g atom	σ, erg/cm^2	S_c, erg/cm^3 K	κ, W/K cm	C_p, J/g K	α_T, cm^2/s
Fe	1809	55.85	6.9	8.09	204	12×10^6	0.39	0.7866	0.072
Ni	1725	58.71	8.0	7.34	255	15.5×10^6	0.469	0.6556	0.089
Pb	600.6	207.21	10.3	20.1	33.3	4.34×10^6	0.165	0.1417	0.106
Sn	505	118.7	6.98	17.0	59	8.53×10^6	0.369	0.2590	0.216
Refs.	periodic table	periodic table	Int. crit. tables	M/ρ		Turnbull	Int. crit. tables	Hultgren et al.[22]	$\kappa/\rho C_p$

Diffusion data: $D_{\text{Ni}-\text{Fe}=4.67\times10^{-5}\text{cm}^2/\text{s}}$
$D_{\text{Pb}\rightarrow\text{Sn}=3.69\times10^{-5}\text{cm}^2/\text{s}}$

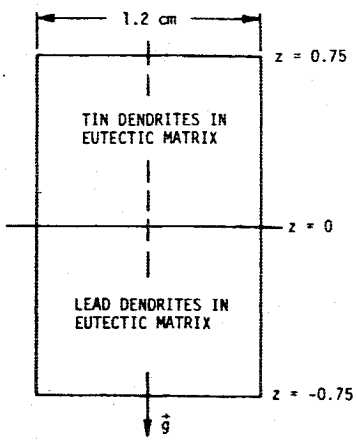

Fig. 3 Sample coordinate system.

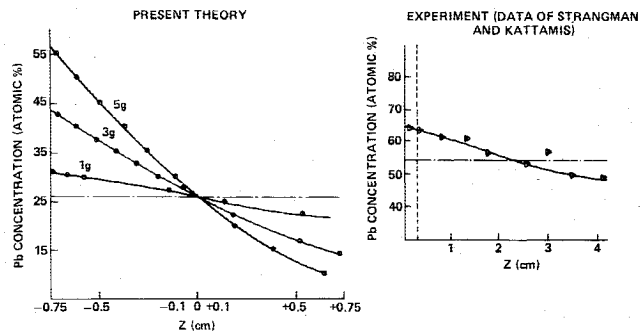

Fig. 4 Concentration vs position.

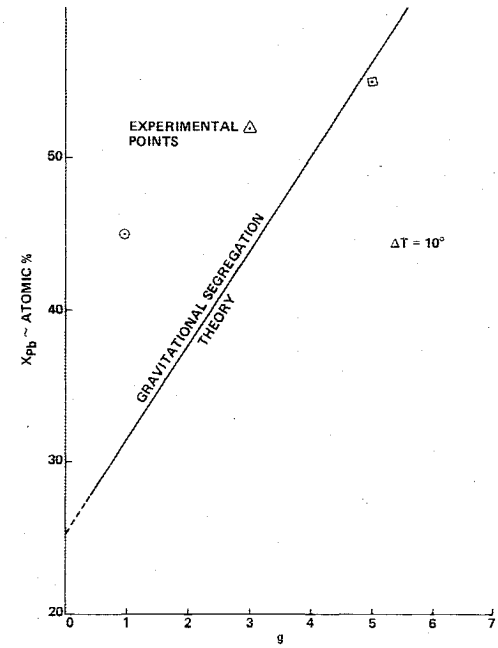

Fig. 5 Gravitational segregation of lead in lead-tin eutectic alloy.

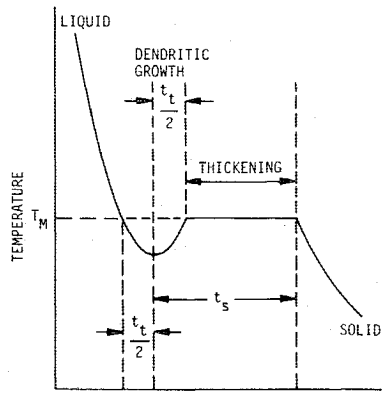

Fig. 6 Solidification cycle.

the MSFC samples, no comparision between theory and the MSFC experiment can be made. However, Strangman and Kattamis[17] performed a similar experiment (at 1 g), and their data are provided for comparison on the right side of Fig. 4. Their material was of a different starting composition from the MSFC samples, complicating comparison. Qualitatively, agreement is good.

The most direct comparison between theory and the MSFC experiments is shown in Fig. 5. Here, atomic fraction is plotted vs gravity for a ΔT of 10 K at a position of $z=-0.75$. Although three data points are not really sufficient to define a curve, it is clear that the postion and slope of any curve through the experimental points would be quite different from those of the theoretical curve. This difference is attributed to the direct undercooling effect exhibited by the original data (Table 1) and not accounted for by the ΔT dependence of γ in Eq. (18).

The hypothesis that observed Pb dendrite segregation is the result of nuclei transport in the melt during a transport time t_t, which is a function of undercooling and during which time the entire melt is undercooled, was tested by estimating the time required for a nucleus moving with velocity

$$U=g\gamma D\{1-[\rho(z)/\rho_{Pb}] \tag{19}$$

to travel a distance of 0.75 cm. The relation of t_t to the rest of the solidification cycle is shown in Fig. 6. For Pb nuclei of mass on the order of 10^{-16} g,

$$\gamma D=(MD/2kT)\approx 2.4\times 10^{-8}\text{s}$$

Thus,

$$t_t=\frac{0.75\text{ cm}}{U}\approx\frac{3\times 10^7}{g[1-\rho(z)/\rho_{Pb}]}$$

For nominal values of g and D, the smallest values of t_t will be for the case of $\rho(z)/\rho_{Pb}\ll 1$. Even then, t_t is on the order of 10^4 s. Since t_s is known experimentally to be approximately 10 to 60 s, depending on g level and undercooling, t_t must be on the order of 10^1 s. This discrepancy invalidates the original hypothesis, if the assumed magnitude of 10^{-5} cm^2/s for the "transport coefficient" D is correct for nuclei this large.

Thus, the mechanism by which undercooling produces the nongravity-related segregation of Pb dendrites observed in the MSFC centrifuge experiments remains a mystery. In fact, the observed increase in segregation with increase is undercooling, seen in Table 1, is contrary to all explanations of melt dynamics considered to date. More effort will be required to explain this anomalous effect.

A Material Property Prediction Model

Since the goal of the space processing program is to create new and/or improved materials, an analytical tool is needed to help determine what new combinations of elements and compositions show enough promise of producing useful materials to warrant experimentation in space and thus to justify the cost of materials experimentation in space. Such a tool is the proposed Material Property Prediction Model (MPPM).

Description of Complete MPPM to be Developed

Figure 7 shows a logic flow diagram for one candidate MPPM. In this model, melt properties such as thermal diffusivity α_T, diffusion coefficient D, liquid-solid interfacial energy σ, entropy of solidification S_c, density ρ, and specific

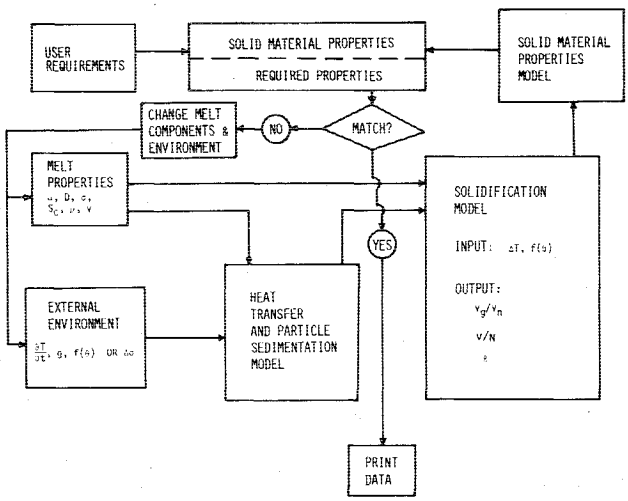

Fig. 7 Comprehensive materials property prediction model.

volume v, together with environmental variables such as cooling rate $\partial T/\partial t$, acceleration (gravity) level g, and heterogeneous nucleation functions $f(\theta)$ or $\Delta\sigma$, which characterize the activity of the nucleants present, are input to the heat-transfer model (to compute melt behavior prior to solidification) and the solidification model, which computes such solid material parameters as grain volume V/N, dendrite arm spacing l, and dendrite morphology parameter v_g/v_n. These parameters may then be used to calculate such solid physical properties as thermal conductivity and thermoelectric power, since these are related to the phonon mean free path which, in turn, depends on the solid microstructure. It may also be possible to calculate mechanical properties of the solid from the microstructural data output from the solidification model. Once the solid properties have been computed, they can be compared to the properties required by the scientific or commercial use to which the solid material is to be put. It is to be expected that an alternative approach could be perfected which would actually derive the required material components and compositions from the user requirements, thus eliminating the trial-and-error required by the candidate MPPM in Fig. 7; but even the trial-and-error calculation would be a great improvement over the present lack of analytical techniques for correlating desired materials properties with component compositions and process environment variables.

The theoretical insights gained in developing the MPPM, which treats gravity as an environmental variable, would also act as a guide for defining materials science experiments which would benefit from the microgravity environment of space. The model would also serve as a microscopic-level materials design tool for application to any processing environment.

Another feature of the MPPM, shown in Fig. 7, is its modularity; the major modules are:

1) The heat transfer and particle sedimentation model, to calculate melt dynamics, including the motion of nucleants (impurities) and nuclei in the melt, and internal thermal characteristics as a function of melt properties and external environmental varibles.

2) Solidification model, to compute the solid microstructural parameters from melt properties, undercooling and nucleant information. It will be discussed in more detail.

3) Solid material properties model, to calculate the properties of the solid material from the microstructure data output from the solidification model. A simple example involves calculation of the thermal conductivity κ from the phonon mean free path Λ by

$$\kappa = \tfrac{1}{3}\bar{v}C_p\Lambda \tag{20}$$

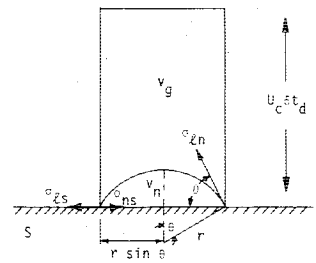

Fig. 8 Simple dendrite—nucleus model.

where $\bar{v}$ is the average phonon velocity in the solid and C_p is heat capacity. The mean free path is on the order of the grain size[18]; thus,

$$\kappa \approx \tfrac{1}{3}\bar{v}C_p\sqrt[3]{V/N} \tag{21}$$

The properties output from the solid properties module are then compared to the desired properties by the remainder of the comprehensive model and, in the candidate MPPM of Fig. 7, the initial melt input is changed and the process repeated, if required.

Discussion of Model Development to Date

The only MPPM module to receive attention thus far is the solidification model. The model as it now exists is based on some crude (simplifying) assumptions which obviously must be replaced by a more realistic picture of the nucleation process. However, this first attempt was made to have a preliminary comparison with experiment (in a limited time) and to ascertain the validity of the MPPM concept. The assumptions and mathematics of the present model will now be given.

Kattamis and Flemings[19] reported observing a distinct change in dendrite morphology as a function of melt undercooling. To describe this theoretically, a "morphology parameter" may be defined, which is simply the ratio of that portion of a dendrite's volume due to growth v_g to the portion which nucleates initially v_n. Figure 8 shows a cylindrical dendrite growing from a spherical cap nucleus formed on a heterogeneous nucleant substrate, characterized by wetting angle θ.

The volume of a spherical cap nucleus is given by[20]

$$v_n = (4/3)\pi r^3 f(\theta) \tag{22}$$

where $f(\theta) = \tfrac{1}{4}(2+\cos\theta)(1-\cos\theta)^2$.

The area of the dendrite base is that of the nucleus and is simply $\pi r^2 \sin^2\theta$. To a close approximation, the dendrite length will be the product of the growth rate U_c with the growing time δt_d, which is the time required for solute atoms to diffuse from the extremities of the region in which a dendrite is growing to the tip of the dendrite. Hence,

$$v_g = \pi r^2 \sin^2\theta U_c \delta t_d \tag{23}$$

Now,

$$r = 2\sigma_{\ell n}/S_c\Delta T \tag{24}$$

and, according to Turnbull,[7,21]

$$U_c = \frac{vDS_c^2}{4\pi kT\sigma_{\ell n}}\Delta T^2 \tag{25}$$

where k is Boltzmann's constant, v is specific volume, and the other symbols are as explained in preceding sections. δt_d is given by

$$\delta t_d = \sqrt{M'/T}(V/N)^{1/3} \tag{26}$$

Table 3 Dendrite morphology correlation

Value of v_g/v_n	Dendrite morphology
$\gg 1$	normal
≈ 1	cylindrical
$\ll 1$	spherical

where V/N is the volume of a grain and

$$M' = \pi m \rho_s a^3 / 48k$$

with

m = solute atom mass
ρ_s = solute atom density
a = solute atom radius

The total volume of material V is assumed known, so the remaining unknown is N, the total number of nuclei which form in the melt. This number is

$$N = IV\delta t_h \tag{27a}$$

or the grain size is

$$V/N = 1/I\delta t_h \tag{27b}$$

where I is the heterogeneous nucleation rate[14]

$$I \cong \exp\{[75.985 - [A^2 f(\theta)/T(\Delta T)^2]\} \tag{28}$$

and δt_h is the time required for heat to flow out of that region of the melt where a single nucleus is forming and is expressed by

$$\delta t_h = (V/N)^{2/3}\sqrt{3/2\alpha_T} \tag{29}$$

where α_T is the thermal diffusivity of the melt. In the present development of a predictive solidification model, Eqs. (26) and (29), the diffusion and heat flow constraints, are derived by dividing the melt into N imaginary cubes. One nucleus is assumed to form at the center of each cube at some time during the interval $\delta t_h < \delta t_d$, which is taken as the total solidification time. The maximum distance which either a solute molecule or heat must travel is that distance from the center of the cube to a corner,

$$\sqrt{3/2}(V/N)^{1/3}$$

Dimensional analysis of the fundamental diffusion and heat flow equations then leads to Eqs. (26) and (29). Equations (22-29) may be solved simultaneously to yield values of all unknown parameters, particularly the morphology v_g/v_n and the grain size V/N. V/N is really the size of each imaginary cube, but its value gives a reasonable indication of average grain size in the solid, and $(V/N)^{1/3}$ is an order-of-magnitude estimate of dendrite spacing. There are three value ranges of v_g/v_n which are of interest, each corresponding to a morphology observed by Kattamis and Flemings (Table 3). This crude mathematical model for calculating grain size and morphology in solids from solidification history contains

Table 4 Solidification model grain size/morphology prediction[a]

ΔT, K	v_g/v_n	ℓ, cm	v_{dendrite}, cm^3	V/N, cm^3
148.0	26.1	1.78	5.1×10^{-19}	5.68
149.0	21.7	1.45	4.2×10^{-19}	3.04
150.0	18.0	1.18	3.5×10^{-19}	1.65
153.4	9.95	0.61	1.9×10^{-19}	0.22
156.0	6.5	0.376	1.2×10^{-19}	5.3×10^{-2}
158.0	4.7	0.26	0.9×10^{-19}	1.8×10^{-2}
160.0	3.5	0.19	6.8×10^{-20}	6.6×10^{-3}
162.5	2.45	0.125	4.9×10^{-20}	1.9×10^{-3}
165.0	1.74	0.084	3.75×10^{-20}	6.0×10^{-4}
167.5	1.26	0.058	2.95×10^{-20}	2.0×10^{-4}
170.0	0.92	0.041	2.4×10^{-20}	6.7×10^{-5}
172.5	0.686	0.03	2.0×10^{-20}	2.4×10^{-5}
175.0	0.517	0.021	1.7×10^{-20}	9.0×10^{-6}
177.5	0.395	0.015	1.5×10^{-20}	3.5×10^{-6}
180.0	0.306	0.011	1.4×10^{-20}	1.4×10^{-6}
182.0	0.25	0.009	1.3×10^{-20}	0.7×10^{-6}
184.0	0.21	0.007	1.2×10^{-20}	3.6×10^{-7}
186.0	0.17	0.0006	1.1×10^{-20}	1.9×10^{-7}
188.0	0.14	0.005	1.06×10^{-20}	1.0×10^{-7}
190.0	0.122	0.0038	1.01×10^{-20}	0.5×10^{-7}
192.0	0.10	0.0031	9.6×10^{-21}	3.0×10^{-8}
194.0	0.088	0.0026	9.2×10^{-21}	1.7×10^{-8}
196.0	0.076	0.0021	8.8×10^{-21}	9.6×10^{-9}
198.0	0.065	0.0018	8.4×10^{-21}	5.6×10^{-9}
200.0	0.057	0.0015	8.1×10^{-21}	3.3×10^{-9}

[a] Material: Fe-.25Ni alloy, wetting angle: $\theta = 81$ deg.

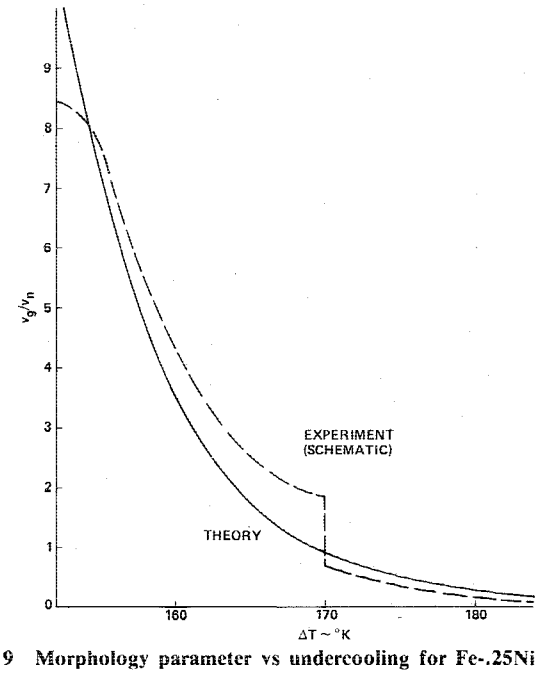

Fig. 9 Morphology parameter vs undercooling for Fe-.25Ni alloy, $\theta = 81$ deg.

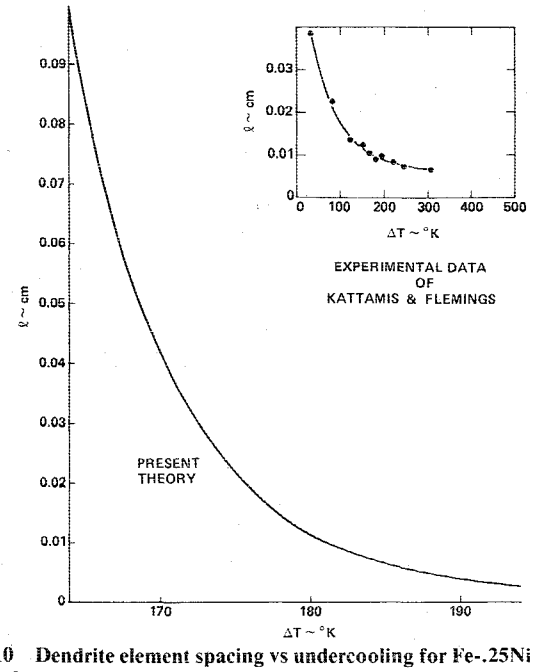

Fig. 10 Dendrite element spacing vs undercooling for Fe-.25Ni alloy, $\theta = 81$ deg.

several simplifying assumptions or deficiencies which should be remedied by more rigorous analyses. The most obvious of these are the following:

1) No account is taken of dendrite branching (other than as a heterogeneous nucleation site for a new dendrite) or of the limiting of one dendrite's growth by other dendrites (except to limit each dendrite to its cube).

2) The heat flow constraint treats only the local (cube) thermal environment, and treats each cube independently; total melt heat-transfer analysis is required.

3) A better definition of total solidification time is required.

4) Model accuracy is no better than the "constant" input parameters used for numerical calculation. At present, very few of the properties of melts required by this model are known with any accuracy.

Although these obstacles are formidible, calculations can be made with the present model which are accurate enough at least to allow comparison with experiment.

Morphology and Grain Size of Fe-.25Ni Alloy

As mentioned previously, Kattamis and Flemings[19] performed the experimental work which established the effect of undercooling on dendrite morphology and grain size. They worked with several alloys, but one which they studied most extensively was Fe-.25Ni. As it happens, the elements Fe and Ni are also two of the few elements, solid at STP, for which all the melt properties required by the previously mentioned mathematical model are either known or can be deduced. Hence, this was the material chosen for comparison between theory and experiment.

The first step was to evaluate all of the constants required by the model equations. Using values of the element properties given in Table 2 for iron and nickel, values of the constants were computed from their defining equations. The model Eqs. (22-29) were then solved simultaneously using the constants and assumed values for the independent variables θ and ΔT. A Wang 700A computer program was written to facilitate calculation of several solid quantities (such as morphology parameter v_g/v_n, dendrite arm spacing l, total dendrite volume $v_{\text{dendrite}} = v_g + v_n$, and grain size V/N) as a function of a wide range of wetting angle and undercooling. Table 4 presents the results of such a calculation for the critical region for the Fe-.25Ni alloy of $\theta = 81$ deg and 148 $K < \Delta T < 200$ K. Kattamis and Flemings had reported a sharp transition from cylindrical to spherical morphology at $\Delta T = 170$ K, hence the interest in this region.

In Figure 9 the theoretical prediction for morphology parameter is plotted beside a schematic representation of Kattamis and Flemings' findings. The general shape of the experimental curve is assumed to be similar to the theoretical, with a discontinuous change of $v_g/v_n > 1$ to $v_g/v_n < 1$ at $\Delta T = 170$ K. To be consistent with Kattamis and Flemings' results, the experimental curve must also remain less than $v_g/v_n \approx 10$ in the interval $30\text{ K} < \Delta T < 170$ K, as is indicated by the onset of asymptotic behavior at approximately $\Delta T = 154$ K in Fig. 9. In Fig. 10, the theoretical and experimental curves for dendrite spacing (or grain diameter) are compared. Although the shapes of the curves are similar, there is a drastic discrepancy between the undercooling scales of the two graphs.

The discrepancies found between the theoretically predicted morphological behavior of Fe-.25Ni alloy during solidification and that which is observed experimentally can be attributed to the simplifying assumptions made to derive the solidification model in its present form, and to the almost complete lack of data for the properties of alloy melts. The facts that v_g/v_n does show a transition from greater than one to less than one at 170 K, albeit a continuous transition, and that the theoretical and experimental curves for dendrite spacing are qualitatively similar provide grounds for hope that an accurate predictive model for alloy solidification behavior (as a function of ΔT and θ) could be developed with sufficient effort. This, in turn, provides confidence that the comprehensive MPPM can and should be developed.

Acknowledgment

The authors are grateful to Carolyn Griner of MSFC and to Paul Lindenmeyer of Boeing for their many helpful suggestions applicable to this work. The work of R. I. Miller was supported by NASA Contract NAS8-31238.

References

[1] Davies, G. J., *Solidification and Casting*, Wiley, New York, 1973.

[2] Winegard, W. C., *An Introduction to the Solidification of Metals*, The Institute of Metals, London, 1964, pp. 1-3, 93-95.

[3] Miller, R. I. and Ruff, R. C., "External Field Effects on Diffusion and Solidification Derived from the Free Volume Model," *Journal of Applied Physics*, Vol. 46, Jan. 1975, pp. 208-212.

[4]Toschev, S., "Homogeneous Nucleation," *Crystal Growth, an Introduction*, North-Holland Publishing Co., Amsterdam, 1973, pp. 1-49.

[5]Jackson, K. A., "Nucleation from the Melt," *Nucleation Phenomena*, American Chemical Society, Washington, 1966, pp. 37-40.

[6]Turnbull, D. and Cohen, M. H., "Crystallization Kinetics and Glass Formation," *Modern Aspects of the Vitreous State*, Vol. 1, Butterworths, Washington, D.C., 1960, pp. 38-62.

[7]Hillig, W. B. and Turnbull, D., "Theory of Crystal Growth in Undercooled Pure Liquids," *Journal of Chemical Physics*, Vol. 24, April 1956, p. 914.

[8]Turnbull, D. and Cech, R. E., "Microscopic Observation of the Solidification of Small Metal Droplets," *Journal of Applied Physics*, Vol. 21, Aug. 1950, pp. 804-810.

[9]Turnbull, D., "The Supercooling of Aggregates of Small Metal Particles," *Journal of Metals*, Vol. 188, Sept. 1950, pp. 1144-1148.

[10]Turnbull, D., "The Undercooling of Liquids," *Scientific American*, Vol. 212, Jan. 1965, pp. 38-46.

[11]Youdelis, W. V. and Iyer, S. P., "Effect of Alloy Composition on Supercooling," *Journal of the Institute of Metals*, Vol. 101, 1973, pp. 176-178.

[12]Iyer, S. P. and Youdelis, W. V., "Effect of Cooling Rate on Supercooling," *Journal of the Institute of Metals*, Vol. 100, 1972, pp. 372-373.

[13]Shiraishi, S. Y. and Ward, R. G., "Undercooling of Nickel," *Canadian Metallurgical Quarterly*, Vol. 3, Jan. 1961, pp. 117-120.

[14]Turnbull, D., "Formation of Crystal Nuclei in Liquid Melts," *Journal of Applied Physics*, Vol. 21, Oct. 1950, pp. 1022-1028.

[15]Glicksman, M. E. and Vold, C. L., "Determination of Absolute Solid-Liquid Interfacial Free Energies in Metals," *Acta Metallurgica*, Vol. 17, Jan. 1969, pp. 1-11.

[16]Johnston, M. H. and Griner, C. S., "Compositional Variations in the Undercooled Pb-Sn Eutectic Solidified at Various Acceleration Levels," *Scripta Metallurgica*, Vol. 11, April 1977, pp. 253-255.

[17]Strangman, T. E. and Kattamis, T. Z., "Gravity Segregation During Remelting of Dendritic Alloys," *Metallurgical Transactions*, Vol. 4, Sept. 1973, pp. 2219-2221.

[18]Ziman, J. M., *Electrons and Phonons*, Oxford Press, 1960, pp. 288-334.

[19]Kattamis, T. Z. and Flemings, M. C., "Dendrite Structure and Grain Size of Undercooled Melts," *Transactions of the Mettalurgical Society of the American Institute of Mining, Metallurgical and Petroleum Engineers*, Vol. 236, Nov. 1966, pp. 1523-1532.

[20]Miller, R. I., "Undercooling of Materials During Solidification in Space," Boeing Aerospace Company, Huntsville, Ala., D256-10202, NASA CR-150011, Aug. 1976.

[21]Turnbull, D. and Cohen, M. H., "Free Volume Model of the Amorphous Phase: Glass Transition," *Journal of Chemical Physics*, Vol. 34, Jan. 1961, pp. 120-125.

[22]Hultgren, R., Orr, R. L., Anderson, P. D., and Kelley, K. K., *Thermodynamic Properties of Metals and Alloys*, Wiley, New York, 1963.